Elastic Properties and Glass Transition of Supported Polymer Thin Films

W. Cheng,*,† R. Sainidou,‡ P. Burgardt,§ N. Stefanou,‡ A. Kiyanova,§ M. Efremov,§ G. Fytas,†,|| and P. F. Nealey§

Max Planck Institute for Polymer Research, P.O. Box 3148, 55128 Mainz, Germany, Section of Solid State Physics, University of Athens, GR-157 84 Athens, Greece, Department of Chemical and Biological Engineering, University of Wisconsin—Madison, Wisconsin 53706, and Department of Materials Science, University of Crete and FO.R.T.H., P.O. Box 1527, GR-711 10 Heraklion, Greece

Received June 1, 2007; Revised Manuscript Received July 20, 2007

ABSTRACT: The present work demonstrates the first application of Brillouin light scattering (BLS) to probe film-guided elastic waves in transparent-substrate supported polymer thin films. In comparison with earlier BLS studies that were restricted to films either free-standing or supported on opaque substrates, the progress made in this work substantially extends the applicability of BLS and permits direct access to the elastic properties of thin films lying on transparent substrates, which is of important practical relevance. A series of thin supported polystyrene and poly(methyl methacrylate) films with thickness in the range of 40−500 nm were explored, and no noticeable trend in elastic properties with thickness has been found, in conformity with earlier BLS results. The first measurement of glass transition temperature, T_g, of supported polymer thin films by BLS is also reported. We observed that the ultrathin (40 nm) films for both polymers exhibit a clear reduction in T_g.

I. Introduction

Polymer thin films with thickness in the range of a hundred of nanometers are extensively used in technological applications such as protective coatings, barrier layers, and optical coatings. In the microelectronic industry, where lithographical patterning of photoresist materials constitutes a critical process, the use of polymer thin films at a sub-100 nm scale is soon anticipated as a result of the continuous demand for miniaturization. For polymer films at such dimensions, especially when the film thickness is approaching the size of the polymer chain, significant deviation in mechanical and thermal properties from those of the bulk may occur,[1] which will exert a considerable impact on their processing and usefulness. For example, capillary forces produced during wet chemical processing of patterned lithographical films can be so strong as to cause the collapse of submicrometer polymeric structures.[2,3] The elastic modulus of thin polymer coatings is of paramount importance in understanding of mechanical instability and collapse of features in lithographic films.[4]

In spite of the ever-growing capability to fabricate nanoscale polymer films, reliable determination of their elastic properties remains an arduous task. The state-of-the-art methods are based on either the mechanical deformation of the thin film[5] or on the acoustic wave propagation within the film.[5−7] The commonly encountered micromechanical methods, such as nanoindentation and atomic force microscopy (AFM), including its modifications, have drawbacks due to the influence of the typically rigid substrate[8] and destructive character of the probe-sample interaction. Other elastic-deformation-based methods including substrate curvature test,[9] bulge test,[10] and buckling-based metrology[11] unavoidably lead to severe damage to the film and sometimes involve complicated sample preparation. Moreover, these mechanical methods usually exhibit poor reproducibility,[5] and the results can show wide variations between laboratories; therefore the determined absolute elastic values should be interpreted with care.

Brillouin light scattering spectroscopy (BLS), featured by its noncontact, nondestructive characteristics, the virtue of requiring uncomplicated sample preparation and high reproducibility, is a powerful tool to extract thermal and mechanical properties of polymer thin films. This technique utilizes inelastic scattering of incident light by thermally activated hypersonic (GHz) elastic waves in the matter. By analyzing the spectral composition of the inelastically scattered light, the information about elastic wave propagation and hence elastic properties of the film can be obtained. BLS is applicable to both supported[6,12,13] and free-standing thin films.[14,15] In the case of supported films, although a substrate is present, its influence on elastic wave propagation is well-defined, in contrast to the mentioned mechanical methods like nanoindentation. In addition, BLS allows easy realization of the study of temperature-dependent elastic properties. Following the change of phase velocity of a given propagation mode with temperature, BLS has been demonstrated to determine the glass transition temperature (T_g) of thin polymer films.[15−17] Thus, as a distinctive method BLS allows integrated determination of elastic properties and T_g of thin polymer films.

A few earlier BLS attempts indicate that the room-temperature high-frequency elastic properties do not exhibit noticeable change for film thickness down to tens of nm.[6,12,13] On the contrary, dramatic decrease in T_g has been found by the same technique for free-standing thin films with thickness below 100 nm.[16,17] There is very limited information about T_g of thin free-standing films from other methods to exclude a technique-dependent T_g determination. Additionally, there are difficulties in applying BLS to probe T_g of supported films due to the dominant scattering signal from a transparent substrate (which is typically much thicker than the probed polymer film) and uncontrolled heating of the sample in the case of opaque substrates.[16]

† Max Planck Institute for Polymer Research.
‡ Section of Solid State Physics, University of Athens.
§ Department of Chemical and Biological Engineering, University of Wisconsin—Madison.
|| Department of Materials Science, University of Crete and FO.R.T.H.

10.1021/ma071227i CCC: $37.00
Published on Web 09/08/2007

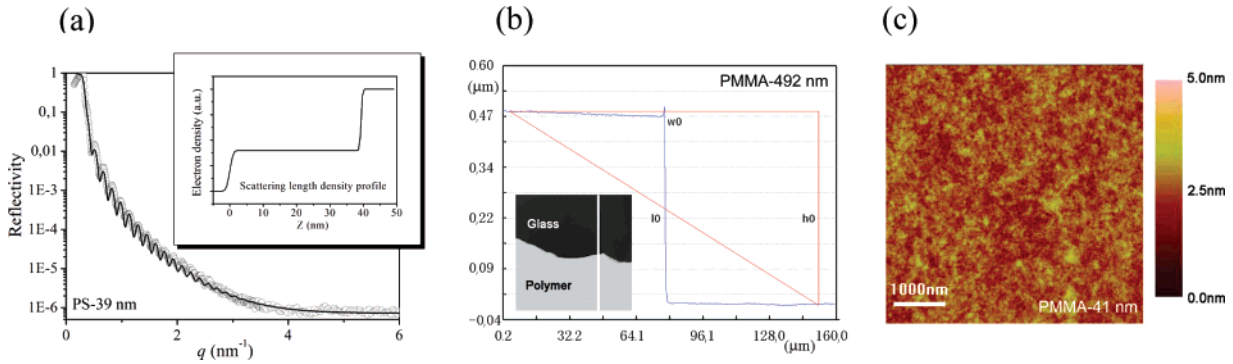

Figure 1. (a) X-ray reflectivity data (open symbols) of the PS-39 film along with the fit (solid curves) using the scattering length density profile shown in the inset. (b) The thickness measurement of the PMMA-492 film using a scanning confocal microscope. (c) Tapping mode AFM image of the surface of the PMMA-41 film.

Table 1. Supported Polystyrene (PS) and Poly(methyl Methacrylate) (PMMA) Films

PS films	PS-39	PS-110	PS-322	PS-514
concn of PS in toluene solution, wt %	1.03	2.35	5.23	7.22
thickness (nm)	39.3 ± 0.3	109.8 ± 0.9	322.2 ± 2.3	514.5 ± 12.3
PMMA films	PMMA-41	PMMA-110	PMMA-320	PMMA-492
concn of PMMA in toluene solution, wt %	1.15	2.43	5.93	7.94
thickness (nm)	40.9 ± 0.3	110.3 ± 1.2	320.4 ± 2.7	491.7 ± 9.8

In this work, we apply a transmission-scattering other than the commonly adopted back-scattering geometry in BLS experiment by virtue of the high-precision goniometer implemented in our apparatus. In combination with the high sensitivity and resolution of the six-path tandem Fabry−Perot interferometer used, we demonstrate that we are able to overcome the signal-masking problem for transparent substrates and realize the integrated BLS determination of elastic properties and T_g of supported thin films. The extension of BLS to optically transparent substrates has the advantage of minimizing the local heating effect, therefore allowing higher laser powers and hence shorter acquisition times. Moreover, such an advancement is important for many applications, e.g., in the field of OLED (organic light emitting devices), where a direct mechanical characterization of thin organic films on transparent substrates is desired. This progress also allows us to check the generality of the BLS results obtained from free-standing thin films. In addition, the introduction of a new method to measure T_g of supported thin films further enriches the tools for studying glass transition under confinement conditions.

II. Experimental Section

A. Film Preparation. Two glass-forming polymers, polystyrene (PS) and poly(methyl methacrylate) (PMMA) with narrow molecular mass distribution, were used in this study. PS (M_w = 61800, M_w/M_n = 1.03) and PMMA (>79% syndiotactic, M_w = 62500, M_w/M_n = 1.04) were purchased from Polymer Source Inc. (samples P4290-S and P2863-MMA, respectively). Microscope cover slides made by optical borosilicate glass were used as substrate (Fisherbrand 25CIR1D), and cleaned before use by oxygen plasma in PE-200 Oxygen Plasma Surface Treatment and Etching System (Plasma Etch) at 50 cm^3/min oxygen flow and 250 W radio frequency power for 10 min.

Thin supported films of PS and PMMA were fabricated by spin-coating of their solutions in toluene on glass substrates at 2000 revolutions per minute for 1 min. Using different polymer solution concentrations (1−8 wt %), thin films with thickness in the range of 40−500 nm were prepared as listed in Table 1. The solutions were filtered through 0.2 μm pore size filters prior to spin-coating. After spin-coating, all films were annealed in a custom-made vacuum furnace at 423 K for 10 h. Nominal residual gas pressure in the furnace was about 100 Pa, and the cooling rate after annealing was about 20 K/h.

B. Film Characterization. The film thickness was measured by a three-wavelength nulling ellipsometer AutoELII on the samples fabricated using the same procedure and sample solutions as stated above except for piranha cleaned silicon wafers were used in place of glass slides. Ellipsometric measurements were verified by X-ray reflectometry and scanning confocal microscopy on selected samples. For film thickness below 120 nm, X-ray reflectrometry (surface XRD-TT3003 diffractometer, SEIFERT) was used, the thickness was obtained by fitting the measured reflectivity curve that shows an oscillatory decay due to Bragg reflection, as shown in Figure 1a for the PS-39 film. For film thickness above 120 nm, a scanning confocal microscope (Nanofocus AG μSurf) equipped with rotating Nipkow disk was employed to directly measure the depth of a scratch on the film made by a sharp needle tip, as illustrated in Figure 1b for the PMMA-492 film. The depth profile in Figure 1b corresponds to the cross section indicated by the white line in the inset, and the thickness was obtained by averaging over the whole sampled area. The surface roughness of these films is rather low, as indicated by the tapping mode AFM (Digital instruments Dimension 3100) image for the PMMA-41 film in Figure 1c.

C. Brillouin Light Scattering (BLS) Spectroscopy. In contrast to the most widely encountered back-scattering geometry[12,13] for film samples, in this work, a special transmission-scattering geometry is used, benefiting from the high-precision goniometer implemented in our setup, which allows easy access to a wide range of scattering angles. The special scattering geometry of Figure 2a with reflection angle α and scattering angle $\theta = 2\alpha$ defines the scattering wave vector **q** with a complete cancellation of the refractive index influence. As a result, $q = (4\pi/\lambda)\sin\alpha$, with λ (=532 nm) being the wavelength of the incident laser beam, does not depend on the refractive index. In addition, for such a scattering geometry, the exchange of the momentum between the photon and the phonon during the scattering process follows the strict instead of the relaxed momentum conservation as requested in the back-scattering geometry which is only favored for light-adsorbing substrates. The inelastically scattered light by the propagating density fluctuations (phonons) with wave vector parallel to the film $\mathbf{k}_{||} = \mathbf{q}$ is analyzed by a high-resolution tandem Fabry−Perot interferometer (FPI)[18] for different q values at hypersonic frequencies ($f \sim 1-50$ GHz). Choosing the polarization of the incident laser beam perpendicular (V) to the scattering plane (perpendicular to the film) and selecting the polarization of the scattered light either perpendicular (V) or parallel (H) to the scattering plane, both polarized (VV) and depolarized (VH) spectra, $I(q,\omega)$, with ω =

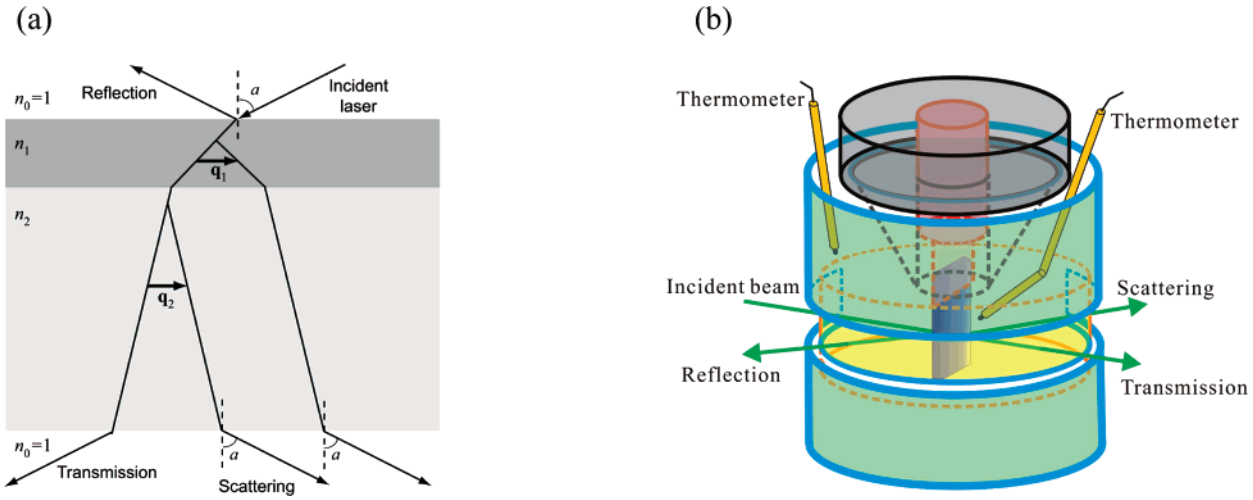

Figure 2. (a) Transmission scattering geometry for recording BLS spectra from a supported film on transparent substrate at a scattering angle twice the incidence angle α. The scattering wave vector **q** is parallel to the film surface. (b) Schematic picture of the sample holder with an optical cell that can be resistively heated, allowing the record of BLS spectra from room temperature up to 473 K.

$2\pi f$, can be recorded. For an isotropic medium these spectra correspond to scattering of light by longitudinal and transverse phonons, respectively. In some experiments, to combine both high resolution and the necessary spectral range, $I(q,\omega)$ at a given q was recorded at two different free spectral ranges (FSR) of the FPI using different mirror separations (see section IV.A).

The sample holder consisting of a cylindrical metallic body and a quartz optical cell also allows BLS measurements at elevated temperatures up to 473 K. The sketch of the holder is shown in Figure 2b. The system is resistively heated, with a 100 Ω platinum RTD temperature sensor embedded in the metallic body to provide feedback for the heater. Another platinum RTD sensor is mounted in close proximity to the sample to obtain the sample temperature. The temperature of the system is stabilized within ±0.2 K. The accumulation time for each spectrum was film thickness dependent, typically 1 h for the thickest film and 10 h for the thinnest film in order to achieve a good signal-to-noise ratio.

All measurements, including those at elevated temperatures, were performed in air. However, no difference in BLS spectrum was detected before and after experiments, implying that the samples were not irreversibly affected (e.g., oxidized) by the surrounding atmosphere.

III. Calculation of Dispersion Diagrams

A homogeneous and isotropic free film supports guided modes of the elastic field. These modes, along any direction parallel to the film, have the form of propagating plane waves with a wave vector $\mathbf{k}_{||}$; along the normal direction, they vanish outside the film on either side of it. The symmetry of the system allows one to separate these modes into two distinct independent classes, according to their polarization: shear horizontal waves with polarization parallel to the film, and waves of mixed longitudinal-transverse character with polarization in the sagittal plane defined by the normal to the film and $\mathbf{k}_{||}$ (Lamb modes).[19] All these modes are, in general, influenced by the presence of elastic media on the two sides of the film, e.g., air and/or a substrate, and, in this case, they are termed Love modes and generalized Lamb modes, respectively.[19] For example, they can leak into the surrounding media. In this case, the guided modes become quasiguided. For the theoretical calculations of the dispersion diagrams associated with the general Lamb (and Love) modes in the supported polymer films studied in this work, we employ the layer-multiple-scattering method which is well documented.[20] This method constitutes a powerful tool for an accurate evaluation of the elastic properties of composite systems consisting of a number of different layers having the same two-dimensional periodicity in the $x-y$ plane (parallel to the layers). An advantage of the method is that it does not require periodicity in the z direction (perpendicular to the layers). For each layer, the method calculates the transmission and reflection matrices $\mathbf{Q}^{\mathrm{I}}$ and $\mathbf{Q}^{\mathrm{III}}$, respectively, for a plane wave incident on the layer with given frequency and $\mathbf{k}_{||}$ from $z \rightarrow -\infty$ (i.e., with $k_z > 0$), as well as the corresponding matrices $\mathbf{Q}^{\mathrm{IV}}$ and $\mathbf{Q}^{\mathrm{II}}$ for incidence from $z \rightarrow \infty$ (i.e., with $k_z < 0$). Explicit expressions for these Q matrices can be found elsewhere.[20] The transmission and reflection matrices of the composite system are calculated from those of the constituent layers. We note that, in the cases considered here, we deal with the simple situation where a layer is a homogeneous plate or a planar interface between two different homogeneous media.

The transmittance, reflectance, and absorbance of a (composite) slab, as well as the corresponding density of states of the elastic field, are obtained from the transmission and reflection matrices of the slab.[20,21] The eigenfrequencies of possible guided modes are evaluated from the condition to have a wave field localized within the slab. Dividing the slab into a left and a right part, this condition leads to the secular equation: $\det[\mathbf{I} - \mathbf{Q}^{\mathrm{II}}(\mathrm{left})\mathbf{Q}^{\mathrm{III}}(\mathrm{right})] = 0$. On the other hand, quasiguided modes of the slab manifest themselves as various types of resonance structures in the corresponding transmission spectrum and as Lorentzian-shaped resonances in the density of states.[22]

IV. Results and Discussion

A. Elastic Properties. Parts a and b of Figure 3 display the polarized BLS spectra of the thinnest and thickest PS and PMMA films recorded at $q = 0.0167$ nm^{-1} at room temperature. The spectra are shown in logarithmic intensity scale to reveal both the strong and weak spectral features in details. For a better visualization, the central elastic feature due to the reference beam[18] was omitted over the frequency range ±3.0 GHz around $f = 0$ GHz. The very intense Brillouin lines at about ±15 GHz in all spectra are due to the strong inelastic light scattering from the bulk longitudinal phonon with $k_{||} = 0.0167$ nm^{-1} in the glass substrate and are therefore independent of the polymer film. The frequency of the glass longitudinal phonon also acts as an internal standard for the scattering wave vector **q**, and the excellent reproducibility of this frequency in Figure 3, parts a and b, indicates the well-defined scattering geometry of the experiment.

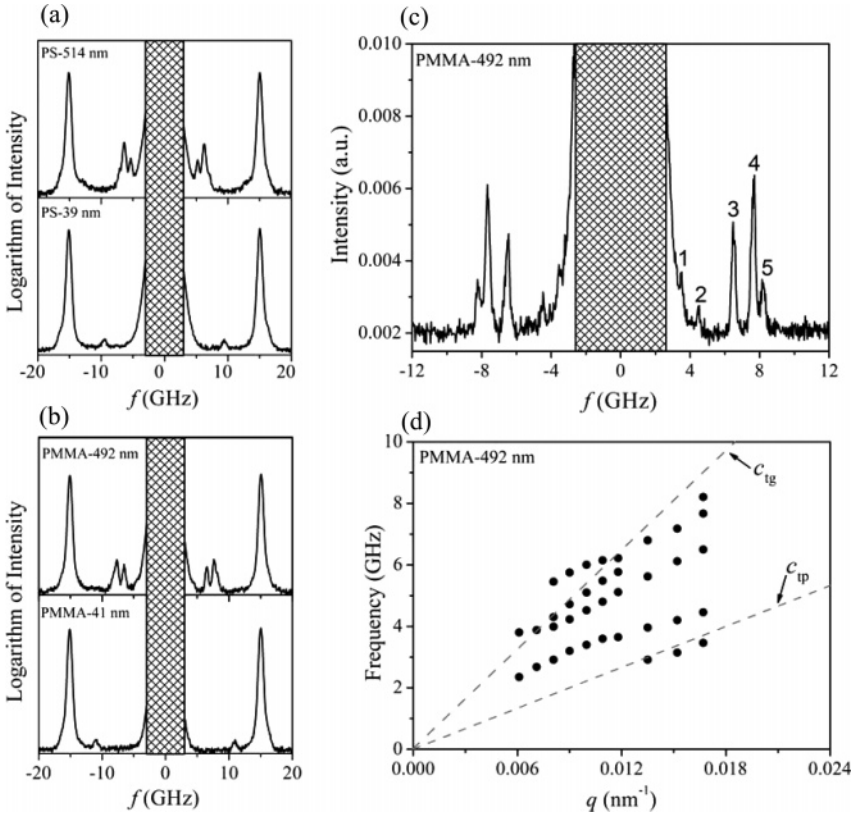

Figure 3. Representative room-temperature BLS spectra of supported PS and PMMA films of different thickness taken at $q = 0.0167$ nm^{-1}. BLS spectra of the PS-514 and PS-39 films (a) and of the PMMA-492 and PMMA-41 films (b) recorded using the free spectral range FSR = 30 GHz. The intense peak centered at around 15 GHz corresponds to the longitudinal phonon in the glass substrate. (c) BLS spectrum ($q = 0.0167$ nm^{-1}) of the PMMA-492 film recorded at a higher resolution (FSR = 15 GHz). It reveals the presence of five peaks. (d) Example of the dispersion relation f vs q for the PMMA-492 film. The two dashed lines indicate the transverse modes in the glass substrate ($c_{tg} = 3390$ m/s) and the bulk PMMA ($c_{tp} = 1400$ m/s).

The observed weaker lines are due to the various film-guided phonons propagating in the supported film configuration with frequencies depending on the polymer species and the film thickness. To resolve closely spaced spectral features, narrower FSR are often needed. For example, the spectrum of the PMMA-492 film in Figure 3c recorded at $q = 0.0167$ nm^{-1} with FSR = 15 GHz reveals additional peaks compared to the spectrum of Figure 3b in which FSR = 30 GHz. The presence of these film-guided modes clearly indicates that the study of elastic excitations in thin supported polymer films on a transparent substrate by BLS is possible in spite of the existence of strong light scattering from the substrate.[16] These surface elastic excitations propagate within the film with different phase velocities $c = \omega_m/k_{||}$, where ω_m ($=2\pi f_m$) is obtained from the position f_m of the spectral peaks, which was determined by fitting the peaks with Lorentzian functions. Identification of the various modes usually proceeds through the calculation of the dispersion relation f vs q which requires q-dependent measurements of $I(q,\omega)$. For example, Figure 3d depicts the dispersion relation for the PMMA-492 film. In contrast to the linear ($f = cq/2\pi$) relationship expected for acoustic-like phonons, the film-guided modes are dispersive (the phase velocity c is not constant), as shown in Figure 3d, and their frequencies roughly fall between the frequencies of the transverse phonons in bulk PMMA and glass, as indicated by the two dashed lines in Figure 3d with phase velocities $c_{tp} = 1400$ m/s and $c_{tg} = 3390$ m/s, respectively.

For elastic wave propagation in thin films, specific forms of dispersion diagrams are often used. The diagrams display the reduced frequency $\omega h/c_{air}$ or the phase velocity $\omega/k_{||}$ as a function of $k_{||}h$, the product of the wave number and the film thickness. The advantage of this representation stems from the fact that for a specific choice of material combination it is the relative magnitude of the wavelength and the film thickness that determine the details of the film-guided modes.[23] It should also be noted that for further discussion we express the elastic properties of the films in terms of longitudinal and transverse phase velocities, instead of the often used Young's modulus and Poisson's ratio. The conversion between them is straightforward with the knowledge of material density.[24] This choice is common in BLS works, as the phase velocities represent the actual measured physical quantities.

The experimental dispersion relations for the supported PS and PMMA thin films of different thicknesses are presented by the symbols in the $\omega/k_{||}$ vs $k_{||}h$ plots in Figure 4, parts a and b, respectively. Following the method described in section III, the theoretical dispersion relations were calculated. In the calculations, the values of the transverse (c_t) and longitudinal (c_l) phase velocities of PS, PMMA, glass and air as well as their densities (ρ) were fixed to the corresponding values of the bulk materials compiled in Table 2. The solid lines in Figure 4, parts a and b, represent the theoretical dispersion relations for the general Lamb modes. It can be seen that very good agreement between theory and experiment is obtained without using any adjustable parameter. On the contrary, the calculated dispersion curves for the corresponding Love modes deviate strongly from the experimental data. Therefore, the comparison between the experimental and theoretical dispersion curves clearly identifies that the observed surface excitations are the general Lamb modes.

Note that in our experiment, the intensity of the first general Lamb mode, or Rayleigh mode (peak 1 in Figure 3c), is rather weak compared to the higher order general Lamb modes, in

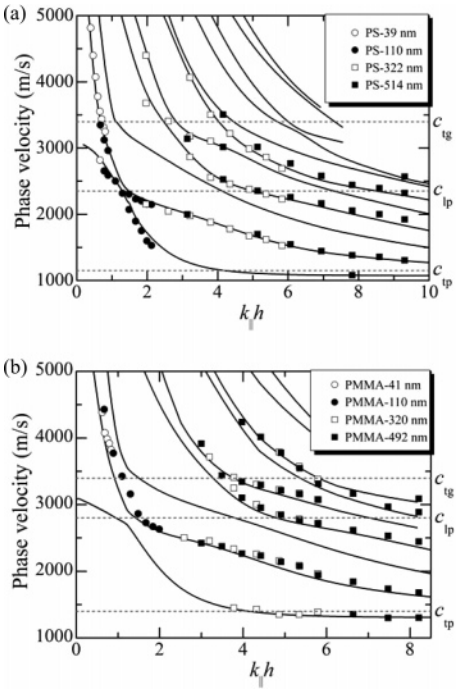

Figure 4. Dispersion diagrams of the phase velocity $c = \omega/k_{||}$ for the different elastic excitations in the supported PS (upper panel) and PMMA (lower panel) thin films presented in the plot of c vs the reduced thickness $k_{||}h$. The solid and open symbols are the experimental points and the solid lines present the theoretical predictions for the general Lamb modes based on the layer-multiple-scattering method with the use of the bulk elastic parameters (Table 2). The short-dashed lines show the phase velocities, c_{tp}, c_{lp}, and c_{tg}, in the different media as described in the text.

Table 2. Bulk Elastic Constants Used in the Theoretical Calculations[a]

material	longitudinal phase velocity, c_l (m/s)	transverse phase velocity, c_t (m/s)	density, ρ (g/cm^3)
PS	2350	1150	1.05
PMMA	2800	1400	1.18
glass	5660	3390	2.50
air	340	0	0.00123

[a] The sound velocities of glass, PS and PMMA are experimental values from the same glass substrate and the two bulk homopolymers.

clear contrast to the very strong Rayleigh mode observed in supported films on opaque substrates.[6,12,25] In the latter case, BLS arises predominantly from surface ripples[26,27] due to the small penetration depth of the incident light. For transparent substrates, the elasto-optical coupling dominates the BLS intensity,[26,27] which increases with the film thickness. It is also noteworthy that, for all the films, the third general Lamb mode is not observed experimentally, possibly due to the weak elasto-optical coupling strength for this mode.

The horizontal short-dashed lines in Figure 4, parts a and b, indicate the transverse phase velocities in both the film and the substrate as well as the longitudinal phase velocity in the polymer. At large $k_{||}h$, the phase velocity of the first general Lamb mode becomes slightly below the polymer transverse phase velocity and approaches asymptotically to the surface Rayleigh velocity of the film material. This is expected because of the much shorter phonon wavelength compared to the film thickness at large $k_{||}h$. It is noteworthy that at smaller $k_{||}h$ many experimental data points are above the glass transverse phase velocity, especially for the thinnest film. General Lamb modes above this transverse threshold, instead of decaying rapidly, show appreciable energy leakage into the substrate,[23] therefore are quasilocalized. Such leaky modes were rarely observed in thin films supported on opaque substrates,[6,12,25] probably due to the dominance of the surface−ripple scattering mechanism. Alternatively their clear manifestation in the present BLS spectra highly suggests that here the intensity is dominated by the strong elasto-optical scattering, which allows detection of the leakage into the transparent substrate. In principle, energy leakage into air is also possible, but the huge acoustic impedance difference makes this leakage negligible. In fact, the theoretical general Lamb modes in Figure 4, parts a and b, remain practically unchanged by replacing air with vacuum. The fairly good description of the experimental general Lamb modes in Figure 4 for all the films of the same material by using a single set of bulk elastic parameters, noticeably with no adjustable parameters, indicates that these films have similar elastic properties as the respective bulk material despite the difference in their thickness. This approach also illustrates the potential of this nondestructive optical technique to measure the elastic parameters of thin films at a selected direction isothermally, e.g., in-plane and out-of-plane.[15]

Next, we make a more accurate estimation of the elastic parameters of these films by allowing variations of the elastic parameters from the bulk values and fitting the data points for different films separately. In the following, the general Lamb modes for the thickest and the thinnest supported PS and PMMA films will be examined. In this case, the comparison between experiment and theory is better shown on the reduced frequency $\omega h/c_{air}$ than on the phase velocity $\omega/k_{||}$ dispersion diagrams. The strategy is to vary c_{tp} and c_{lp} relatively to the bulk values and seek for the best agreement with the experiment. For the thinnest films, the experiment probes the beginning (small $k_{||}h$) of the lower branches of the general Lamb modes, and it is found that these branches are rather insensitive to moderate variations of c_{lp}. Consequently for the thinnest films, we kept c_{lp} to the bulk value and adjusted c_{tp} to achieve the best agreement between theory and experiment. On the contrary, for the thickest films, in addition to the lower branches, higher branches are also probed experimentally. It turns out that the latter are sensitive to the change of c_{lp}, thus the fitting procedure requests both c_{lp} and c_{tp} to be adjusted for a good fit of both the lower and higher branches.

Parts a and b of Figure 5 refer to the optimal fitting results for the PS-39 and PS-514 films, respectively. For the ultrathin PS-39 film, the best capture of the two lowest branches can be achieved by increasing c_{tp} by 6% (c_{tp} = 1220 m/s) relative to the bulk PS value (Table 2). The five branches observed for the PS-514 film can be well represented by allowing c_{lp} and c_{tp} to be 2.5% higher (c_{lp} = 2410 m/s and c_{tp} = 1180 m/s) than the bulk values. To better visualize the elastic difference between them, the lowest two branches of the general Lamb modes in Figure 5b are also shown in Figure 5a as indicated by the dashed lines. Similar procedures are applied to the PMMA films, and the fits are shown in Figure 5, parts c and d. In the case of the PMMA-41 film, an 8% higher c_{tp} (c_{tp} = 1510 m/s) is used, while for the PMMA-492 film an increase of both c_{lp} and c_{tp} by 4% (c_{lp} = 2910 m/s and c_{tp} = 1455 m/s) is necessary. Therefore, the experimental results show that within about 4% error, c_{lp} and c_{tp} assume the same values in the thickness range of about 40−500 nm for both supported thin PS and PMMA films, respectively. Considering that the experimental error amounts to about 2%, the observed 4% difference is not significant. In other words, no notable change in high frequency (in the GHz range) mechanical properties has been found in these thin supported polymer films in the glassy state with

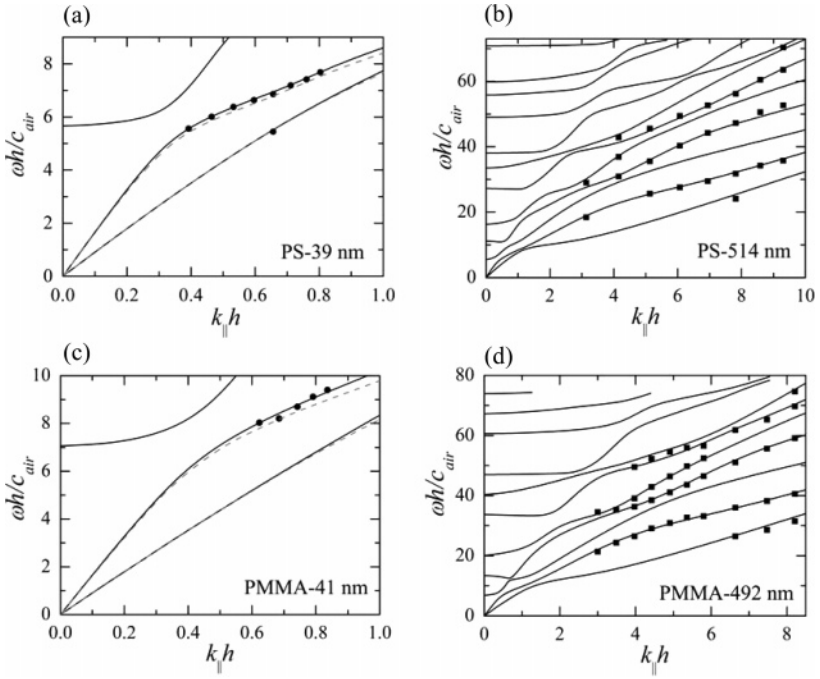

Figure 5. Dispersion diagrams presented in the plot of reduced frequency $\omega h/c_{air}$ vs $k_{||}h$ for both the PS and PMMA films of two extreme thickness values: PS-39 (a), PS-514 (b), PMMA-41 (c), and PMMA-492 (d). The symbols are experimental points and the lines present the optimal fits using fixed values for the elastic constants of the glass substrate but adjustable c_{lp} and c_{tp} of the polymer films. The dashed lines in Figure 5a (c) are the magnification of the lowest two branches in Figure 5b (d).

thickness down to at least 40 nm. A widely accepted phenomenological picture of the glassy state leads to the relation[28] $c_{lp} \propto (v_0/v_f)^{1/3}$, where v_f is the free volume defined by $v_f = v - v_0$, the difference between the specific volume v and the closest packing volume v_0. Invariable c_{lp} for different thicknesses for both polymers would imply that either the packing or the ratio v_0/v_f does not depend on the thickness of the films under investigation. Our data confirm previous BLS results on thin films supported on light-absorbing substrates,[6,12,13] and are also in agreement with a recent experiment finding based on buckling-based metrology,[11] which operates at low frequencies.

Investigation of polymer samples thinner than 40 nm is limited by the sensitivity of our current BLS design. The elasto-optical contribution to the signal is proportional to the probed sample volume. Hence a thinner film yields a weaker scattering signal. Additionally, the dispersion relations imply that the phase velocity of the probed phonons in the thinner film will become closer to that of the glass longitudinal phonon, which makes the weak polymer peak in the spectrum hardly resolvable.

B. Glass Transition. The successful detection of the general Lamb modes makes the study of the glass transition of thin supported polymer films by BLS possible. In this case the complication brought about by substrate heating effect is no longer present and T_g can be estimated from the distinctly different temperature dependence of phase velocities in the glassy and rubbery states. The phase velocity of any general Lamb mode as a function of temperature can be used for glass transition observation, as demonstrated for the free-standing thin films.[16,17] Temperature-dependent measurements were carried out by heating the sample situated in the heating chamber from room temperature to 413 K in successive steps. At each given temperature the sample was stabilized for about 10 min before the beginning of the measurements.

In this work, only the thickest and thinnest films of both polymers were subjected to glass transition investigation. There are two reasons for this choice. First, many existing experimental results suggest that deviation of T_g from the bulk value starts to appear when the film thickness becomes below 100 nm.[1] Second, the central goal of this study is to demonstrate that BLS technique is capable of probing the glass transition in a few tens of nanometer thick supported polymer films. To our knowledge, it has never been shown before. Figure 6 displays the BLS spectrum of PS-514 at given $q = 0.0152$ nm^{-1}, at 11 different temperatures in the glassy and rubbery states. Significant change in the spectra upon heating of the sample is clearly seen. The two dashed lines indicate the position of two strong modes at room temperature for guidance. The corresponding velocity vs temperature functions are shown in Figure 7a. Transition from the glassy state to the rubbery one is clearly marked by a kink on the plots. The T_g is assigned as the temperature of the intersection of the least-square-fit-determined glass and liquid straight lines, and highlighted by the shadowed

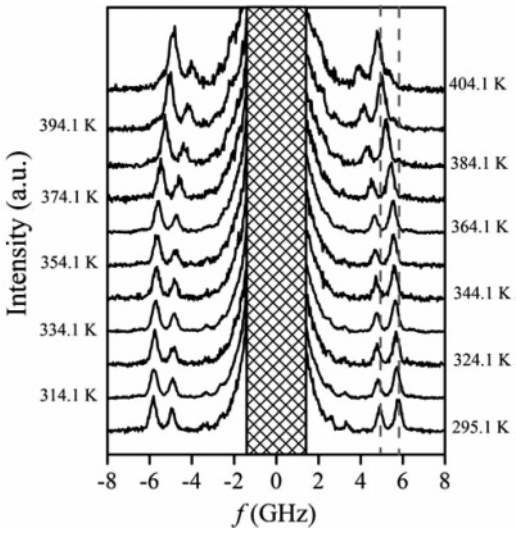

Figure 6. BLS spectra for the PS-514 film at $q = 0.0152$ nm^{-1} at 11 different temperatures below and above T_g. The spectra are shifted for clarity. The glass transition can be studied by monitoring the change of the peak frequency with temperature.

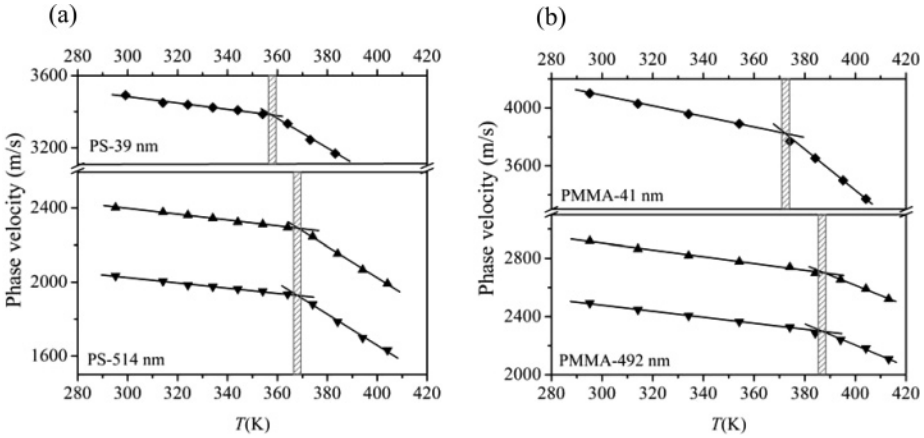

Figure 7. Phase velocities of a few general Lamb modes (at constant q) propagating in the PS (a) and PMMA (b) films with two extreme thickness values were plotted as a function of temperature by heating up the film from room temperature to 413 K in successive steps. The symbols are the experimental points and the solid lines denote the linear least-square fits for the glassy and rubbery states intersecting at the glass transition temperature, as indicated by the shaded region. For the thicker films, the two strongest general Lamb modes are chosen, and for the thinner films, the only observable general Lamb mode is utilized.

regions in Figure 7. For the thickest PS-514 and PMMA-492 (Figure 7b) films, the determined T_g values are 368 ± 0.3 and 387 ± 0.3 K, respectively. T_g for bulk samples (6−10 mg) of the same polymers was measured using differential scanning calorimetry (DSC). A Q100 DSC tool (TA Instruments) was used. The temperature program contains three cycles of heating/cooling in the range 293−433 K for PS and 293−453 K for PMMA. Both heating and cooling rates are 1 K/min. The data for T_g measurement are collected upon cooling. T_g was assigned using the limiting fictive temperature concept. Found T_g values for PS and PMMA are 372.6 and 395.8 K, respectively. T_g measured by BLS for the thickest PS and PMMA films are slightly lower than the calorimetric values (by 5 and 9 K respectively) but still in reasonable agreement with them. The results for the thinnest films are also presented in Figure 7. A clear T_g depression (10 K for PS-39 and 15 K for PMMA-41) is observed in both ultrathin films regardless of their different chemical nature.

One of the instrumental factors that can be partially responsible for the decreased T_g in BLS experiments (especially for thin films) is the significant data accumulation time (as much as 10 h for thin films—see section II.C). Because of the kinetic nature of glass transition, its temperature region depends on the time frame of the measurement. When the time frame increases, the transition temperature region shifts to lower temperatures.[29] For measurements upon heating, this phenomenon also can be discussed in terms of physical aging. We examine the influence of physical aging on the experimental results within the typical time frame of our BLS measurements as follows. A piece of 1 mm thick free-standing polystyrene sheet (M_w = 280 000, M_w/M_n = 2.5, Goodfellow Ltd.) was heated at a rate 10 K/min from room temperature to 353.1 K. After reaching 353.1 K (t = 0 min), two BLS spectra were recorded at t = 10 min and t = 12 h with 2 min accumulation time for each. Such short accumulation times were permitted by the thickness of the sample. As demonstrated in Figure 8, the two spectra are experimentally the same, thus implying that physical aging can be ignored for our experiments at least up to 20 K below T_g. The interpolation base for the glass line on the velocity vs temperature plots is much wider than the 20 K T_g vicinity region, so the position of the glass line is not affected by physical aging. The same procedure was repeated at 388.1 K, which is near but above T_g. In the equilibrium rubbery state, the spectra in Figure 8 confirm the expected insensitivity to the equilibration time. In conclusion, the above-mentioned experiment shows that the influence of the data accumulation time on the T_g assignment is negligible within the experimental time scale used. This statement is supported by the previous BLS works: quantitative agreement between slow BLS measurements of free-standing polymer films and transmission ellipsometry measurements made on much shorter time scales, shown elsewhere.[30]

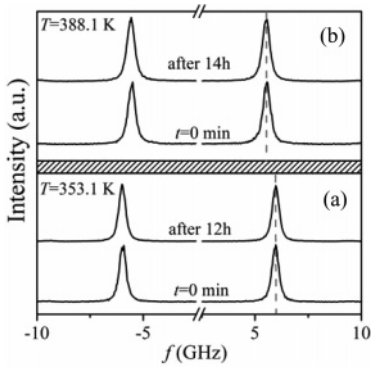

Figure 8. BLS spectra of a bulk (1 mm thick) PS sheet recorded at two different annealing times at two temperatures: (a) below and (b) above T_g.

This notion of softening of ultrathin films at lower temperatures compared to the bulk material is corroborated by the values of the elastic constants of the thinnest films at temperatures near but above T_g. For example, at 374.1 K, using the experimental data for the PS-39 and PS-514 films, c_{lp} and c_{tp} are found to, compared to their respective room-temperature values, decrease by about 26% and 13% for the PS-39, and 22% and 6% for the PS-514. The stronger softening for the PS-39 film is in conformity to its lower T_g. The 10 K reduction in T_g for the PS-39 film agrees with many existing experimental results.[31,32] For those experiments where T_g depression is observed, PS thin films typically demonstrate negative deviation of T_g, whatever kind of substrate is used.[31] T_g depression is thought to be the indicator of the weak interaction between the polymer and the substrate.[33] For the PMMA-41 film, the clearly observed 15 K decrease in T_g did not follow our expectation, as the formation of hydrogen bond between PMMA and the silicon oxide surface is supposed to lead to a higher energy barrier for segmental motion and therefore to an increase in T_g[31,34]. It should be mentioned that the PMMA system is much less extensively investigated than the PS, no reliable conclusion can be made so far and contradictory results exist.[35,36] For

PMMA thin films, it is found that tacticity also plays a role. For example, isotactic PMMA on Si substrate exhibits strong decrease in T_g with decreasing film thickness, while syndiotactic PMMA demonstrates the opposite trend on the same substrate.[37]

As it was pointed out above, a detailed glass transition investigation is beyond the scope of this work. Rather, the aim is to demonstrate that BLS technique is able to clearly observe glass transition in 40 nm thick supported polymer films. It is interesting also, that no direct correlation between the room-temperature elastic properties of the thin films under investigation and the change in their T_g has been found in our work. It agrees with previous study in free-standing films, where no deviation from the bulk elastic parameters has been found for a reduction in T_g as much as 65 K[14].

V. Conclusions

With the use of a transmission-scattering geometry, we demonstrated for the first time that BLS can be applied to probe elastic properties of thin polymer films with thickness down to 40 nm supported on transparent substrates, despite of the intense light scattering from the substrate. The longitudinal and transverse phase velocities measured at room temperature (c_{lp} and c_{tp}) are found to be practically the same for both PS and PMMA films with thickness in the range of 40−500 nm. Our results confirm earlier BLS studies employing opaque substrates. The use of transparent substrates eliminates the uncontrollable heating effect present for opaque substrates, which means that the BLS measurement of T_g can be extended from free-standing to supported films. For both PS and PMMA ultrathin (∼40 nm) films, a clear decrease in T_g was observed in spite of the different chemical nature of the two polymers and the subsequently expected different interactions between the polymer and the substrate surface. Our data also indicate that in the case of transparent substrates different mechanism is responsible for the scattering intensity from the surface elastic waves. The recorded BLS spectra are therefore valuable for justifying the validity of theoretical models that attempt to elucidate the elasto-optical coupling in the scattering process.

Acknowledgment. We thank Dr. J. S. Gutmann at the Max Planck Institute for Polymer Research for the X-ray reflectivity measurements.

References and Notes

(1) Roth, C. B.; Dutcher, J. R. Mobility on different length scales in thin polymer films. In *Soft materials (structure and dynamics*); Dutcher, J. R.; Marangoni, A. G., Eds.; Marcel Dekker: New York, 2005.
(2) Cao, H. B.; Nealey, P. F.; Domke, W. D. *J. Vac. Sci. Technol. B* **2000**, *18*, 3303−3307.
(3) Stoykovich, M. P.; Cao, H. B.; Yoshimoto, K.; Ocola, L. E.; Nealey, P. F. *Adv. Mater.* **2003**, *15*, 1180−1184.
(4) Hartschuh, R.; Ding, Y.; Roh, J. H.; Kisliuk, A.; Sokolov, A. P.; Soles, C. L.; Jones, R. L.; Hu, T. J.; Wu, W. L.; Mahorowala, A. P. *J. Polym. Sci., Part B: Polym. Phys.* **2004**, *42*, 1106−1113.
(5) Jansen, K. M. B.; Gonda, V.; Ernst, L. J. *J. Electron. Packag.* **2006**, *127*, 530.
(6) Sun, L.; Dutcher, J. R.; Giovannini, L.; Nizzoli, F.; Stevens, J. R.; Ord, J. L. *J. Appl. Phys.* **1994**, *75*, 7482−7488.
(7) Rogers, J. A.; Maznev, A. A.; Banet, M. J.; Nelson, K. A. *Annu. Rev. Mater. Sci.* **2000**, *30*, 117−157.
(8) Kovalev, A.; Shulha, H.; M.; L.; Myshkin, N.; Tsukruk, V. V. *J. Mater. Res.* **2004**, *19*, 716−728.
(9) Zhao, J. H.; Ryan, T.; Ho, P. S.; Mckerrow, A. J.; Shih, W. Y. *J. Appl. Phys.* **2000**, *88*, 3029−3038.
(10) Zheng, D. W.; Xu, Y. H.; Tsai, Y. P.; Tu, K. N.; Patterson, P.; Zhao, B.; Liu, Q. Z.; Brongo, M. *Appl. Phys. Lett.* **2000**, *76*, 2008−2010.
(11) Stafford, C. M.; Vogt, B. D.; Harrison, C.; Julthongpiput, D.; Huang, R. *Macromolecules* **2006**, *39*, 5095−5099.
(12) Forrest, J. A.; Rowat, A. C.; Dalnoki-Veress, K.; Stevens, J. R.; Dutcher, J. R. *J. Polym. Sci., Part B: Polym. Phys.* **1996**, *34*, 3009−3016.
(13) Hartschuh, R. D.; Kisliuk, A.; Novikov, V.; Sokolov, A. P.; Heyliger, P. R.; Flannery, C. M.; Johnson, W. L.; Soles, C. L.; Wu, W. L. *Appl. Phys. Lett.* **2005**, *87*, 173132.
(14) Forrest, J. A.; Dalnoki-Veress, K.; Dutcher, J. R. *Phys. Rev. E* **1998**, *58*, 6109−6114.
(15) Cheng, W.; Gorishnyy, T.; Krikorian, V.; Fytas, G.; Thomas, E. L. *Macromolecules* **2006**, *39*, 9614−9620.
(16) Forrest, J. A.; Dalnoki-Veress, K.; Dutcher, J. R. *Phys. Rev. E* **1997**, *56*, 5705−5716.
(17) Forrest, J. A.; Dalnoki-Veress, K.; Stevens, J. R.; Dutcher, J. R. *Phys. Rev. Lett.* **1996**, *77*, 2002−2005.
(18) Penciu, R. S.; Kriegs, H.; Petekidis, G.; Fytas, G.; Economou, E. N. *J. Chem. Phys.* **2003**, *118*, 5224−5240.
(19) Auld, B. A. *Acoustic fields and waves in solids*; Wiley: New York, 1973; Vol. II.
(20) Sainidou, R.; Stefanou, N.; Psarobas, I. E.; Modinos, A. *Comput. Phys. Commun.* **2005**, *166*, 197−240.
(21) Sainidou, R.; Stefanou, N.; Modinos, A. *Phys. Rev. B* **2004**, *69*, 064301.
(22) Sainidou, R.; Stefanou, N. *Phys. Rev. B* **2006**, *73*, 184301.
(23) Farnell, G. W.; Adler, E. L.; Elastic wave propagation in thin layers. In *Physical acoustics, principles and methods*; Mason, W. P., Thurston, R. N., Eds.; Academic Press: New York, 1972.
(24) Landau, L. D.; Lifshitz, E. M. *Theory of elasticity*, 3rd ed.; Reed Educational and Professional: Oxford, U.K., 1986.
(25) Wittkowski, T.; Distler, G.; Jung, K.; Hillebrands, B.; Comins, J. D. *Phys. Rev. B* **2004**, *69*, 205401.
(26) Loudon, R. *J. Phys. C: Solid State Phys.* **1978**, *11*, 2623−2637.
(27) Loudon, R. *Phys. Rev. Lett.* **1978**, *40*, 581−583.
(28) Champion, J. V.; Jackson, D. A. *Mol. Phys.* **1976**, *31*, 1159−1168.
(29) Wunderlich, B. *Assignment of the Glass Transition*; ASTM STP 1249; American Society for Testing and Materials: Philadelphia, PA, 1994.
(30) Dalnoki-Veress, K.; Forrest, J. A.; Murray, C.; Gigault, C.; Dutcher, J. R. *Phys. Rev. E* **2001**, *63*, 031801.
(31) Forrest, J. A.; Dalnoki-Veress, K. *Adv. Colloid Interface Sci.* **2001**, *94*, 167−196.
(32) Kawana, S.; Jones, R. A. L. *Phys. Rev. E* **2001**, *63*, 021501.
(33) Fryer, D. S.; Peters, R. D.; Kim, E. J.; Tomaszewski, J. E.; de Pablo, J. J.; Nealey, P. F.; White, C. C.; Wu, W. *Macromolecules* **2001**, *34*, 5627−5634.
(34) Hartmann, L.; Gorbatschow, W.; Hauwede, J.; Kremer, F. *Eur. Phys. J. E* **2002**, *8*, 145−154.
(35) Reiter, G.; Forrest, J. *Eur. Phys. J. E* **2002**, *8*, 101−101.
(36) Yamamoto, S.; Tsujii, Y.; Fukuda, T. *Macromolecules* **2002**, *35*, 6077−6079.
(37) Grohens, Y.; Hamon, L.; Reiter, G.; Soldera, A.; Holl, Y. *Eur. Phys. J. E* **2002**, *8*, 217−224.

MA071227I